Three-point combined compact alternating direction implicit difference schemes for two-dimensional time-fractional advection-diffusion equations

Guang-Hua Gao[1] and Hai-Wei Sun[2]*

[1] *College of Science, Nanjing University of Posts and Telecommunications, Nanjing 210046, P. R. China.*
[2] *Department of Mathematics, University of Macau, Macao*

Abstract. This paper is devoted to the discussion of numerical methods for solving two-dimensional time-fractional advection-diffusion equations. Two different three-point combined compact alternating direction implicit (CC-ADI) schemes are proposed and then, the original schemes for solving the two-dimensional problems are divided into two separate one-dimensional cases. Local truncation errors are analyzed and the unconditional stabilities of the obtained schemes are investigated by Fourier analysis method. Numerical experiments show the effectiveness and the spatial higher-order accuracy of the proposed methods.

AMS subject classifications: 65M06, 65M12, 65N06, 65N12

Key words: Time-fractional advection-diffusion equations, Combined compact difference (CCD) scheme, ADI, Stability, Fourier analysis.

1 Introduction

Fractional calculus has been widely studied recently since its numerous practical applications have not been realized until a couple of last decades [1]. It has found increasing place in wide field of applications including control system community, turbulent flows, viscoelasticity, plasma physics, thermodynamics, anomalous diffusion in porous media, finance theory and so on. These applications prompted the emergence of various fractional differential equations in mathematical and physical world [1–3]. To seek the solutions of these equations becomes an essential part of mathematicians' work. The integral transform method, power series method and Green's function method are employed to produce the analytical solution of some fractional differential equations. Consequently, the solution usually refers to some special functions which are quite complicated in real calculation. Numerical solutions of fractional differential equations are preferred by many scholars.

*Corresponding author. *Email addresses:* gaoguanghua1107@163.com (G. Gao), hsun@umac.mo (H. Sun)

The time-fractional derivative is used to describe the stochastic process with non-Markovian property, or the anomalous diffusion process with memory. The differential equation with presence of the time-fractional derivative is called the time-fractional differential equation. The huge amount of works focused on how this class of equation is numerically solved, among which the finite difference method was extensively applied. For one-dimensional time-fractional differential equations, Yuste and Acedo [4], Langlands and Henry [5], Chen et al. [6], Sun and Wu [7] developed various finite difference methods with the second-order accuracy in space. To promote the spatial accuracy, some fourth-order compact finite difference methods were proposed successively. Cui [8], Gao and Sun [9], Zhang, Sun and Wu [10], Mohebbi and Abbaszadeh [11] focused on the study of spatial fourth-order accurate finite difference methods for solving the time-fractional subdiffusion equations. More relevant works cover the literatures by Du, Cao and Sun [12] for the second-order fractional wave equation, Hu and Zhang [13] for the fourth-order diffusion-wave system, Ren and Sun [14] for the second-order fractional wave equation with Neumann boundary conditions. In addition, the finite difference discretization in time and spectral approximation in space was reported in [15] for time-fractional diffusion equations.

As we know, the time-fractional derivative is nonlocal operator of convolution type. Values on current time level depend on values on all previous time levels. The variable storage and computational cost appear an increasing burden as time grows, especially during simulating long time behaviors of solutions. Hence, it is worth developing some higher-order accurate numerical methods for solving the time-fractional differential equations. For high dimensional problems, this requirement is more outstanding. Some relevant works have been done along this way. For two-dimensional anomalous sub-diffusion equations, Brunner, Ling and Yamamoto [16] discussed an algorithm by coupling an adaptive time stepping and adaptive spatial basis selection approach. Chen et al. [17] proposed two numerical methods for this problem: one was implicit and the other was explicit, based on Grünwald-Letnikov approximation for the time-fractional derivative. Fourier analysis method was used to discuss their stability and convergence. Recently, the ADI technique was introduced to handle the two-dimensional time-fractional differential equations. Zhang and Sun [18] presented two different ADI schemes for the 2D time-fractional subdiffusion equation. The stability and convergence of the resulting schemes were analyzed by the discrete energy method. The obtained schemes in [17, 18] were both second-order accurate in space. To improve the numerical accuracy, Cui [19, 20] investigated high-order compact ADI schemes for the 2D time-fractional sub-diffusion equation. Zhang, Sun and Zhao [21], Zhang and Sun [22] constructed compact difference schemes for the 2D time-fractional wave equation and sub-diffusion equation, respectively. It is worthwhile to note that all these compact schemes achieve the fourth-order accuracy in space.

In the present work, the new compact and spatial higher-order accurate numerical methods will be established for solving the two-dimensional time-fractional differential equations. For this purpose, the combined compact difference (CCD) technique presented by Chu and Fan in [23] is recalled here. The first-order derivatives, the second-order derivatives and unknown function values are joined together to be computed in this method. The

computational cost, albeit unknowns included increased, will not become a bottleneck of the method itself since only a small stencil is involved. This is just one of the fascinating facets of the CCD method. Another important feature of the CCD method lies in that the high-order accurate evaluation of the first- and second-order derivatives of unknowns can provide vital information for the post-processing, especially for some singular value problems. More refined meshes can be introduced, where the derivative values are relatively big, to promote the efficiency of numerical methods. Until now, the CCD method has been successfully used for solving the one-dimensional Burgers' equation [24], two-dimensional Navier-Stokes equations [25], problem of thermal convection and convection-driven dynamo in a rotating spherical shell [26], two-dimensional convection-diffusion equation [27] and so on. More details on CCD can be found in [23, 28–31].

As the authors' known, the applications of the CCD technique into the fractional differential equations have never been found except our first attempt to discuss the one-dimensional time-fractional advection-diffusion equations (TFADEs) by the CCD method in [32], where the effective numerical schemes were proposed and strict theoretical analysis of the resultant scheme for constant coefficient case with periodic boundary conditions was also given. Now this paper aims to extend the idea to solve the two-dimensional time-fractional advection-diffusion equations. At the same time, the original schemes for solving the two-dimensional case are divided into two separate one-dimensional ones by using the ADI techniques. The computational complexity is reduced to some extent. By adding some proper perturbation terms just similar to that in [18], two different kinds of combined compact ADI schemes are presented and strict stability analysis for these schemes is investigated by the Fourier method.

The remainder of this paper is arranged as follows. In Section 2, two different kinds of combined compact ADI (CC-ADI) difference schemes are presented to solve the two-dimensional TFADEs by adding different perturbation terms. Strict stability analysis of these two schemes is given by the Fourier method. Numerical experiments are illustrated in Section 3, which show the effectiveness, robustness and spatial high-order accuracy of these numerical schemes. A brief conclusion is included in Section 4.

2 The CC-ADI difference schemes for TFADEs

In the section, the following two-dimensional TFADEs will be considered.

$$
\begin{aligned}
{}_0^C\mathcal{D}_t^\alpha u(x,y,t) &= \kappa_1 u_{xx}(x,y,t)+\kappa_2 u_{yy}(x,y,t)-pu_x(x,y,t)-qu_y(x,y,t)+f(x,y,t),\\
&\qquad (x,y)\in\mathbb{R}^2,\ t\in(0,T], \qquad (2.1)\\
u(x,y,0) &= u_0(x,y), \quad (x,y)\in\mathbb{R}^2, \qquad (2.2)
\end{aligned}
$$

subject to the (d_1,d_2)-periodic boundary conditions

$$
u(x,y,t)=u(x+d_1,y,t),\ u(x,y,t)=u(x,y+d_2,t) \quad (x,y)\in\mathbb{R}^2,\ t\in[0,T], \qquad (2.3)
$$

where $\kappa_1,\kappa_2,p,q,\ d_1,d_2,\alpha$ are all constants, $\kappa_1,\kappa_2>0,\ d_1,d_2>0,\ 0<\alpha<1$ and ${}_0^C\mathcal{D}_t^\alpha$ is the α-th Caputo fractional derivative defined by

$$ {}_0^C\mathcal{D}_t^\alpha g(t)=\frac{1}{\Gamma(1-\alpha)}\int_0^t \frac{g'(s)}{(t-s)^\alpha}\mathrm{d}s. $$

For numerical approximation, the time grid partition is firstly given. For any positive integer N, denote $t_k=k\tau$ with $\tau=T/N$, $k=0,1,\ldots,N$. For any discrete grid function $v=\{v^k\,|\,0\leqslant k\leqslant N\}$, define

$$ D_t^\alpha v^k=\frac{\tau^{-\alpha}}{\Gamma(2-\alpha)}\left[a_0^{(\alpha)}v^k-\sum_{l=1}^{k-1}(a_{k-l-1}^{(\alpha)}-a_{k-l}^{(\alpha)})v^l-a_{k-1}^{(\alpha)}v^0\right], \tag{2.4} $$

with

$$ a_j^{(\alpha)}=(j+1)^{1-\alpha}-j^{1-\alpha},\quad j\geqslant 0. \tag{2.5} $$

Usually, D_t^α is called the L1 approximation operator for the Caputo time-fractional derivative operator ${}_0^C\mathcal{D}_t^\alpha$, which is derived from a piecewise linear approximation of function $v(t)$. The following lemma shows that the numerical accuracy of this approximation is $\mathcal{O}(\tau^{2-\alpha})$ if $v(t)\in C^2[0,t_k]$.

Lemma 2.1. *[7] Suppose $v(t)\in C^2[0,t_k]$. Then it holds that*

$$ \left|{}_0^C\mathcal{D}_t^\alpha v(t)|_{t=t_k}-D_t^\alpha v(t_k)\right|\leqslant\frac{1}{\Gamma(2-\alpha)}\left[\frac{1-\alpha}{12}+\frac{2^{2-\alpha}}{2-\alpha}-(1+2^{-\alpha})\right]\max_{0\leqslant t\leqslant t_k}|v''(t)|\tau^{2-\alpha}, $$

where $0<\alpha<1$ and D_t^α is defined by (2.4).

Secondly, for solving the periodic initial-boundary value problem (2.1)–(2.3), one can restrict it on a space bounded domain $\Omega=(0,d_1]\times(0,d_2]$. For any two positive integers M and N, denote $x_i=ih_x,y_j=jh_y$ with $h_x=d_1/M_1,h_y=d_2/M_2,0\leqslant i\leqslant M_1+1,0\leqslant j\leqslant M_2+1$. Denote $\Omega_h=\{(x_i,y_j)\,|\,1\leqslant i\leqslant M_1,1\leqslant j\leqslant M_2\}$ and $\Omega_h^E=\{(x_i,y_j)\,|\,0\leqslant i\leqslant M_1+1,0\leqslant j\leqslant M_2+1\}$.

Suppose $u(x,y,t)\in C^{8,8,2}(\Omega\times[0,T])$. Define the grid functions

$$ U_{ij}^k=u(x_i,y_j,t_k),\ (U_x)_{ij}^k=u_x(x_i,y_j,t_k),\ (U_{xx})_{ij}^k=u_{xx}(x_i,y_j,t_k),\ (U_y)_{ij}^k=u_y(x_i,y_j,t_k), $$

$$ (U_{yy})_{ij}^k=u_{yy}(x_i,y_j,t_k),\quad f_{ij}^k=f(x_i,y_j,t_k),\ 0\leqslant i(j)\leqslant M_1(M_2)+1,\ 0\leqslant k\leqslant N. $$

Denote

$$ \mathcal{L}_x:=\kappa_1\frac{\partial^2}{\partial x^2}-p\frac{\partial}{\partial x},\ \mathcal{L}_y:=\kappa_2\frac{\partial^2}{\partial y^2}-q\frac{\partial}{\partial y}. $$

2.1 The three-point CC-ADI difference scheme (*CC-ADI-L1* scheme)

Considering Eq. (2.1) at point (x_i,y_j,t_k), it yields from the L1 approximation for time-fractional derivative that

$$D_t^\alpha U_{ij}^k=\mathcal{L}_x U_{ij}^k+\mathcal{L}_y U_{ij}^k+f_{ij}^k-(R_t)_{ij}^k,\quad (x_i,y_j)\in\Omega_h,\ 1\leqslant k\leqslant N, \tag{2.6}$$

where $(R_t)_{ij}^k={}_0^C\mathcal{D}_t^\alpha U_{ij}^k-D_t^\alpha U_{ij}^k$. By Lemma 2.1, it holds that $(R_t)_{ij}^k=\mathcal{O}(\tau^{2-\alpha})$.

In order to reduce the computational complexity, the ADI technique is employed. To aim that, a small term $\mu^2 D_t^\alpha\mathcal{L}_x\mathcal{L}_y U_{ij}^k$ is added to the left hand side of (2.6) with $\mu=\tau^\alpha\Gamma(2-\alpha)$ and it leads to

$$D_t^\alpha\left(U_{ij}^k+\mu^2\mathcal{L}_x\mathcal{L}_y U_{ij}^k\right)=\mathcal{L}_x U_{ij}^k+\mathcal{L}_y U_{ij}^k+f_{ij}^k+(\overline{R_t})_{ij}^k,\quad (x_i,y_j)\in\Omega_h,\ 1\leqslant k\leqslant N, \tag{2.7}$$

where $(\overline{R_t})_{ij}^k=\mu^2 D_t^\alpha\mathcal{L}_x\mathcal{L}_y U_{ij}^k-(R_t)_{ij}^k=\mathcal{O}\left(\tau^{\min\{2-\alpha,2\alpha\}}\right)$. Neglecting the small term $(\overline{R_t})_{ij}^k$ and rearranging the result, it produces

$$\begin{aligned}(I-\mu\mathcal{L}_x)(I-\mu\mathcal{L}_y)u_{ij}^k=&\sum_{l=1}^{k-1}\left(a_{k-l-1}^{(\alpha)}-a_{k-l}^{(\alpha)}\right)\left(u_{ij}^l+\mu^2\mathcal{L}_x\mathcal{L}_y u_{ij}^l\right)+a_{k-1}^{(\alpha)}\left(u_{ij}^0+\mu^2\mathcal{L}_x\mathcal{L}_y u_{ij}^0\right)\\&+\mu f_{ij}^k,\quad (x_i,y_j)\in\Omega_h,\ 1\leqslant k\leqslant N.\end{aligned} \tag{2.8}$$

For the purpose of deriving the CCD scheme for solving (2.1)–(2.3) on the space domain Ω, two expressions for any function $g(x)\in C^8[x_{i-1},x_{i+1}]$ associated with its first- and second-order derivatives are recalled as [23]

$$\frac{7}{16}(g'_{i+1}+g'_{i-1})+g'_i-\frac{h}{16}(g''_{i+1}-g''_{i-1})=\frac{15}{16h}(g_{i+1}-g_{i-1})+\mathcal{O}(h^6), \tag{2.9}$$

$$\frac{9}{8h}(g'_{i+1}-g'_{i-1})-\frac{1}{8}(g''_{i+1}+g''_{i-1})+g''_i=\frac{3}{h^2}(g_{i+1}-2g_i+g_{i-1})+\mathcal{O}(h^6), \tag{2.10}$$

with $x_i-x_{i-1}=x_{i+1}-x_i=h$ and $g_i=g(x_i)$, $g'_i=g'(x_i)$, $g''_i=g''(x_i)$.

Multiplying Eq. (2.9) by $8/15$, one can obtain

$$\frac{1}{30}(7g'_{i+1}+16g'_i+7g'_{i-1})=\frac{g_{i+1}-g_{i-1}}{2h}+\frac{h^2}{15}\frac{g''_{i+1}-g''_{i-1}}{2h}+\mathcal{O}(h^6). \tag{2.11}$$

The left hand side of the above equality is an average of the values of function $g'(x)$ at three points. The Eq. (2.11) can be explained as follows: Approximate

$$\frac{1}{30}(7g'_{i+1}+16g'_i+7g'_{i-1})$$

by

$$\frac{g_{i+1}-g_{i-1}}{2h}+\frac{h^2}{15}\frac{g''_{i+1}-g''_{i-1}}{2h}$$

with the sixth-order accuracy. Similarly, multiplying Eq. (2.10) by 4/3, one has

$$-\frac{1}{6}g''_{i-1}+\frac{4}{3}g''_i-\frac{1}{6}g''_{i+1}=4\frac{g_{i+1}-2g_i+g_{i-1}}{h^2}-3\frac{g'_{i+1}-g'_{i-1}}{2h}+\mathcal{O}(h^6).$$

The left hand side of the above equality is an average of the values of function $g''(x)$ at three points. And the above equality means that the approximating

$$-\frac{1}{6}g''_{i-1}+\frac{4}{3}g''_i-\frac{1}{6}g''_{i+1}$$

by

$$4\frac{g_{i+1}-2g_i+g_{i-1}}{h^2}-3\frac{g'_{i+1}-g'_{i-1}}{2h}$$

has the accuracy of six order.

Hence, a CC-ADI difference scheme for solving (2.1)–(2.3) can be obtained together with the application of (2.9)–(2.10) for $u(x,y,t_k)$ both in x-direction and y-direction. In this way, the original difference scheme for solving the two-dimensional problem can be divided into two separate one-dimensional CCD scheme. More precisely, for all $(x_i,y_j)\in\Omega_h, 1\leqslant k\leqslant N$, firstly, implementing computation in x-direction on time level $t=t_*$ in the following manner:

$$\begin{cases}(I-\mu\mathcal{L}_x)u^*_{ij}=\sum\limits_{l=1}^{k-1}\left(a^{(\alpha)}_{k-l-1}-a^{(\alpha)}_{k-l}\right)\left(u^l_{ij}+\mu^2\mathcal{L}_x\mathcal{L}_y u^l_{ij}\right)+a^{(\alpha)}_{k-1}\left(u^0_{ij}+\mu^2\mathcal{L}_x\mathcal{L}_y u^0_{ij}\right)+\mu f^k_{ij},\\ \frac{7}{16}[(u_x)^*_{i+1,j}+(u_x)^*_{i-1,j}]+(u_x)^*_{ij}-\frac{h_x}{16}[(u_{xx})^*_{i+1,j}-(u_{xx})^*_{i-1,j}]=\frac{15}{16h_x}\left(u^*_{i+1,j}-u^*_{i-1,j}\right),\\ \frac{9}{8h_x}[(u_x)^*_{i+1,j}-(u_x)^*_{i-1,j}]-\frac{1}{8}[(u_{xx})^*_{i+1,j}+(u_{xx})^*_{i-1,j}]+(u_{xx})^*_{ij}=\frac{3}{h_x^2}(u^*_{i+1,j}-2u^*_{ij}+u^*_{i-1,j}),\end{cases}\tag{2.13}$$

where $\{u^*_{ij}\},\{(u_x)^*_{ij}\},\{(u_{xx})^*_{ij}\}$ are intermediate values used for computation, $u^0_{ij}=u_0(x_i,y_j)$ for all $(x_i,y_j)\in\Omega_h$.

Secondly, going on computing in y-direction on time level $t=t_k$ with respect to the unknowns $\{u^k_{ij}\},\{(u_y)^k_{ij}\},\{(u_{yy})^k_{ij}\}$ as follows:

$$\begin{cases}(I-\mu\mathcal{L}_y)u^k_{ij}=u^*_{ij},\\ \frac{7}{16}\left[(u_y)^k_{i,j+1}+(u_y)^k_{i,j-1}\right]+(u_y)^k_{ij}-\frac{h_y}{16}\left[(u_{yy})^k_{i,j+1}-(u_{yy})^k_{i,j-1}\right]=\frac{15}{16h_y}\left(u^k_{i,j+1}-u^k_{i,j-1}\right),\\ \frac{9}{8h_y}\left[(u_y)^k_{i,j+1}-(u_y)^k_{i,j-1}\right]-\frac{1}{8}\left[(u_{yy})^k_{i,j+1}+(u_{yy})^k_{i,j-1}\right]+(u_{yy})^k_{ij}=\frac{3}{h_y^2}\left(u^k_{i,j+1}-2u^k_{ij}+u^k_{i,j-1}\right).\end{cases}\tag{2.14}$$

Here, the difference scheme (2.13)–(2.14) is denoted as *CC-ADI-L1* scheme. The coefficient matrices of (2.13) and (2.14) are both triple-tridiagonal and they can be solved according to the algorithm proposed in [23], namely, first, triple-forward elimination and then,

triple-backward substitution. In addition, the computation for $\mathcal{L}_x\mathcal{L}_y u_{ij}^l$ can be referred to the detailed algorithm described in [27], which was carried out by two steps: first, compute the values of $\mathcal{L}_y u_{ij}^l$ from u_{ij}^l by (2.9)–(2.10) after neglecting the small term $\mathcal{O}(h^6)$, then, proceed the similar procedure to obtain the values of $\mathcal{L}_x\mathcal{L}_y u_{ij}^l$ based on the obtained values $\mathcal{L}_y u_{ij}^l$ using (2.9)–(2.10) again after neglecting the small term $\mathcal{O}(h^6)$.

2.2 Analysis of the *CC-ADI-L1* scheme

In this section, the stability of difference scheme (2.13)–(2.14) will be concerned by the Fourier analysis. Suppose

$$u_{ij}^*=\xi^*(m_1,m_2)e^{\mathbf{i}(iw_x+jw_y)},\ (u_x)_{ij}^*=\xi_x^*(m_1,m_2)e^{\mathbf{i}(iw_x+jw_y)},\ (u_{xx})_{ij}^*=\xi_{xx}^*(m_1,m_2)e^{\mathbf{i}(iw_x+jw_y)},$$

$$(u_y)_{ij}^*=\xi_y^*(m_1,m_2)e^{\mathbf{i}(iw_x+jw_y)},\ (u_{yy})_{ij}^*=\xi_{yy}^*(m_1,m_2)e^{\mathbf{i}(iw_x+jw_y)},\ f_{ij}^*=\eta^*(m_1,m_2)e^{\mathbf{i}(iw_x+jw_y)},$$

where $\mathbf{i}=\sqrt{-1}$, $w_x=2m_1\pi h_x/d_1$, $w_y=2m_2\pi h_y/d_2$ and t^* denotes any time level $(0\leqslant t^*\leqslant t_N)$. By the Parseval identity, we know

$$\|u^k\|^2:=h_xh_y\sum_{i=1}^{M_1}\sum_{j=1}^{M_2}(u_{ij}^k)^2=d_1d_2\sum_{m_1,m_2}|\xi^k(m_1,m_2)|^2,\ 0\leqslant k\leqslant N,$$

and the other norms, such as $\|f^k\|^2$, can be defined similarly. In the following, we simply omit m_1,m_2 without ambiguity.

First, several lemmas are needed in order to facilitate the analysis of difference scheme (2.13)–(2.14).

Lemma 2.2. *[9] Suppose $0<\alpha<1$ and $a_j^{(\alpha)}$ is defined by* (2.5)*, $j=0,1,2,\ldots$. Then*

(1) $1=a_0^{(\alpha)}>a_1^{(\alpha)}>a_2^{(\alpha)}>\cdots>a_j^{(\alpha)}\to 0$, as $j\to+\infty$;

(2) $a_{k-1}^{(\alpha)}>(1-\alpha)k^{-\alpha}$.

Lemma 2.3. *[27, 32] For any t_* $(t_{k-1}<t_*<t_k)$ and t_k $(1\leqslant k\leqslant N)$, it holds*

$$\begin{cases}\xi_x^*=\mathbf{i}\dfrac{1}{h_x}\phi(\cos w_x,\sin w_x)\xi^*,\\ \xi_{xx}^*=\dfrac{1}{h_x^2}\psi(\cos w_x)\xi^*,\end{cases}\quad\begin{cases}\xi_y^k=\mathbf{i}\dfrac{1}{h_y}\phi(\cos w_y,\sin w_y)\xi^k,\\ \xi_{yy}^k=\dfrac{1}{h_y^2}\psi(\cos w_y)\xi^k,\end{cases}\tag{2.15}$$

where

$$\phi(x,y)=\frac{9y(4+x)}{2x^2+20x+23},\quad \psi(x)=\frac{3(11x^2+8x-19)}{2x^2+20x+23}.$$

Remark: The lemma can be easily proved using the latter two equalities of (2.13)–(2.14), respectively.

Theorem 2.1. *The CC-ADI scheme* (2.13)–(2.14) *is unconditionally stable with respect to the initial values and source terms. More precisely, it holds*

$$\|u^k\|^2 \leqslant 2\|u^0\|^2 + 2T^{2\alpha}\Gamma^2(1-\alpha)\max_{1\leqslant l\leqslant N}\|f^l\|^2, \quad 1\leqslant k\leqslant N. \tag{2.16}$$

Proof. From (2.8) and Lemma 2.3, we get

$$\begin{aligned}(1-a_x-\mathbf{i}b_x)(1-a_y-\mathbf{i}b_y)\xi^k = &\sum_{l=1}^{k-1}\left(a_{k-l-1}^{(\alpha)}-a_{k-l}^{(\alpha)}\right)\left[1+(a_x+\mathbf{i}b_x)(a_y+\mathbf{i}b_y)\right]\xi^l\\ &+a_{k-1}^{(\alpha)}\left[1+(a_x+\mathbf{i}b_x)(a_y+\mathbf{i}b_y)\right]\xi^0+\mu\eta^k, 1\leqslant k\leqslant N,\end{aligned} \tag{2.17}$$

where

$$\begin{aligned}a_x &= \kappa_1\frac{\mu}{h_x^2}\psi(\cos w_x),\ b_x = -p\frac{\mu}{h_x}\phi(\cos w_x,\sin w_x),\\ a_y &= \kappa_2\frac{\mu}{h_y^2}\psi(\cos w_y),\ b_y = -q\frac{\mu}{h_y}\phi(\cos w_y,\sin w_y).\end{aligned}$$

A straightforward calculation can be carried out to show that $\psi(x)\leqslant 0$ for $x\in[-1,1]$, hence $a_x\leqslant 0, a_y\leqslant 0$. Noticing $|(1-a_x-\mathbf{i}b_x)(1-a_y-\mathbf{i}b_y)|\geqslant 1$ and

$$\begin{aligned}&|(1-a_x-\mathbf{i}b_x)(1-a_y-\mathbf{i}b_y)|^2-|1+(a_x+\mathbf{i}b_x)(a_y+\mathbf{i}b_y)|^2\\ =&[(1-a_x)(1-a_y)-b_xb_y]^2+[b_x(1-a_y)+b_y(1-a_x)]^2\\ &-(1+a_xa_y-b_xb_y)^2-(a_xb_y+a_yb_x)^2\\ =&(a_x+a_y)^2-2(a_x+a_y)(1+a_xa_y)+(b_x+b_y)^2-2(a_xb_y^2+a_yb_x^2)\\ \geqslant&0,\end{aligned}$$

namely,

$$|1+(a_x+\mathbf{i}b_x)(a_y+\mathbf{i}b_y)|\leqslant|(1-a_x-\mathbf{i}b_x)(1-a_y-\mathbf{i}b_y)|, \tag{2.18}$$

by (2.17) and Lemma 2.2, we get

$$|\xi^k|\leqslant\sum_{l=1}^{k-1}\left(a_{k-l-1}^{(\alpha)}-a_{k-l}^{(\alpha)}\right)|\xi^l|+a_{k-1}^{(\alpha)}|\xi^0|+\mu|\eta^k|, \quad 1\leqslant k\leqslant N.$$

In addition, by Lemma 2.2, noting

$$\mu=\tau^\alpha\Gamma(2-\alpha)=(k\tau)^\alpha\Gamma(1-\alpha)k^{-\alpha}(1-\alpha)<T^\alpha\Gamma(1-\alpha)a_{k-1}^{(\alpha)},$$

it follows

$$|\xi^k|\leqslant\sum_{l=1}^{k-1}\left(a_{k-l-1}^{(\alpha)}-a_{k-l}^{(\alpha)}\right)|\xi^l|+a_{k-1}^{(\alpha)}(|\xi^0|+T^\alpha\Gamma(1-\alpha)|\eta^k|), \quad 1\leqslant k\leqslant N. \tag{2.19}$$

Squaring both sides of the inequality (2.19), by Cauchy-Schwarz inequality, we have

$$\begin{aligned}|\xi^k|^2 \leqslant & \Big[\sum_{l=1}^{k-1}\Big(a_{k-l-1}^{(\alpha)}-a_{k-l}^{(\alpha)}\Big)\cdot 1^2+a_{k-1}^{(\alpha)}\cdot 1^2)\Big] \\ & \bullet\Big[\sum_{l=1}^{k-1}\Big(a_{k-l-1}^{(\alpha)}-a_{k-l}^{(\alpha)}\Big)|\xi^l|^2+a_{k-1}^{(\alpha)}(2|\xi^0|^2+2T^{2\alpha}\Gamma^2(1-\alpha)|\eta^k|^2)\Big] \\ = & \sum_{l=1}^{k-1}\Big(a_{k-l-1}^{(\alpha)}-a_{k-l}^{(\alpha)}\Big)|\xi^l|^2+a_{k-1}^{(\alpha)}(2|\xi^0|^2+2T^{2\alpha}\Gamma^2(1-\alpha)|\eta^k|^2), \quad 1\leqslant k\leqslant N,\end{aligned}$$

hence,

$$\|u^k\|^2 \leqslant \sum_{l=1}^{k-1}\Big(a_{k-l-1}^{(\alpha)}-a_{k-l}^{(\alpha)}\Big)\|u^l\|^2+a_{k-1}^{(\alpha)}(2\|u^0\|^2+2T^{2\alpha}\Gamma^2(1-\alpha)\|f^k\|^2), \quad 1\leqslant k\leqslant N. \tag{2.20}$$

Define

$$F=2\|u^0\|^2+2T^{2\alpha}\Gamma^2(1-\alpha)\max_{1\leqslant l\leqslant N}\|f^l\|^2,$$

it follows from (2.20) that

$$\|u^k\|^2 \leqslant \sum_{l=1}^{k-1}\Big(a_{k-l-1}^{(\alpha)}-a_{k-l}^{(\alpha)}\Big)\|u^l\|^2+a_{k-1}^{(\alpha)}F, \quad 1\leqslant k\leqslant N. \tag{2.21}$$

Then the estimate inequality (2.16) can be directly derived from (2.21) by mean of the mathematical induction method. The proof ends. □

2.3 Another three-point CC-ADI difference scheme (*CC-ADI-BD* scheme)

In this section, another three-point CC-ADI difference scheme for solving (2.1)–(2.3) is proposed, which will be denoted as *CC-ADI-BD* scheme. The slight difference between the *CC-ADI-L1* scheme (2.13)–(2.14) and the *CC-ADI-BD* scheme lies in that a different perturbation term is added to Eq. (2.6). To derive the *CC-ADI-BD* scheme, a small term $\mu\mathcal{L}_x\mathcal{L}_y(U_{ij}^k-U_{ij}^{k-1})$ is added to the both hand sides of (2.6), we get

$$D_t^\alpha U_{ij}^k+\mu\mathcal{L}_x\mathcal{L}_y(U_{ij}^k-U_{ij}^{k-1})=\mathcal{L}_xU_{ij}^k+\mathcal{L}_yU_{ij}^k+f_{ij}^k+(\widehat{R}_t)_{ij}^k, \quad (x_i,y_j)\in\Omega_h,\ 1\leqslant k\leqslant N, \tag{2.22}$$

where

$$(\widehat{R}_t)_{ij}^k=\mu\mathcal{L}_x\mathcal{L}_y(U_{ij}^k-U_{ij}^{k-1})-(R_t)_{ij}^k=\mathcal{O}(\tau^{\min\{1+\alpha,2-\alpha\}}).$$

Omitting the small term $(\widehat{R}_t)_{ij}^k$ in (2.22) and multiplying the result by μ bring to

$$(I-\mu\mathcal{L}_x)(I-\mu\mathcal{L}_y)u_{ij}^k=\mu^2\mathcal{L}_x\mathcal{L}_yu_{ij}^{k-1}+\sum_{l=1}^{k-1}(a_{k-l-1}^{(\alpha)}-a_{k-l}^{(\alpha)})u_{ij}^l$$

$$+a_{k-1}^{(\alpha)}u_{ij}^0+\mu f_{ij}^k,\quad (x_i,y_j)\in\Omega_h,\ 1\leqslant k\leqslant N. \tag{2.23}$$

Similar to the idea of *CC-ADI-L1* decomposition, Eq. (2.23) together with (2.9)–(2.10) and the initial value condition can be computed in the following ADI way:

For the computation of unknown function $u(x,y,t)$ on $t=t_k$, firstly, on an intermediate time level t_*, compute $\{u_{ij}^*\},\{(u_x)_{ij}^*\},\{(u_{xx})_{ij}^*\}$ in x-direction as follows:

$$\begin{cases}(I-\mu\mathcal{L}_x)u_{ij}^*=\mu^2\mathcal{L}_x\mathcal{L}_y u_{ij}^{k-1}+\sum\limits_{l=1}^{k-1}(a_{k-l-1}^{(\alpha)}-a_{k-l}^{(\alpha)})u_{ij}^l+a_{k-1}^{(\alpha)}u_{ij}^0+\mu f_{ij}^k,\\ \dfrac{7}{16}[(u_x)_{i+1,j}^*+(u_x)_{i-1,j}^*]+(u_x)_{ij}^*-\dfrac{h_x}{16}[(u_{xx})_{i+1,j}^*-(u_{xx})_{i-1,j}^*]=\dfrac{15}{16h_x}[u_{i+1,j}^*-u_{i-1,j}^*],\\ \dfrac{9}{8h_x}[(u_x)_{i+1,j}^*-(u_x)_{i-1,j}^*]-\dfrac{1}{8}[(u_{xx})_{i+1,j}^*+(u_{xx})_{i-1,j}^*]+(u_{xx})_{ij}^*=\dfrac{3}{h_x^2}(u_{i+1,j}^*-2u_{ij}^*+u_{i-1,j}^*).\end{cases} \tag{2.24}$$

Secondly, the computation in y-direction is carried out in the same way as (2.14).

Eq. (2.24) with (2.14) is the new CC-ADI difference scheme for solving (2.1)–(2.3), denoted by the *CC-ADI-BD* scheme. The algorithm of solving (2.24) and (2.14) is just like what for the *CC-ADI-L1* scheme (2.13)–(2.14).

2.4 Analysis of the *CC-ADI-BD* scheme

The stability of the *CC-ADI-BD* scheme (2.24) and (2.14) is analyzed in this part. For this purpose, a lemma is given first.

Lemma 2.4. *For any two complex numbers z_1, z_2 with $Re(z_1)\leqslant 0$ and $Re(z_2)\leqslant 0$, it holds*

$$|(1-z_1)(1-z_2)|-|z_1z_2|\geqslant 1, \tag{2.25}$$

where $Re(z)$ denotes the real part for any complex number z.

Proof. Since $Re(z_1)\leqslant 0$ and $Re(z_2)\leqslant 0$, let $z_1=re^{\mathbf{i}\theta_1}$, $z_2=\rho e^{\mathbf{i}\theta_2}$ with $r=|z_1|$, $\rho=|z_2|$, θ_1 and θ_2 the argument of z_1 and z_2, respectively. Apparently it holds that $\cos\theta_1\leqslant 0$ and $\cos\theta_2\leqslant 0$. Observing that

$$\begin{aligned}&|(1-z_1)(1-z_2)|^2-(|z_1z_2|+1)^2\\ =&|1-r\cos\theta_1-\mathbf{i}r\sin\theta_1|^2|1-\rho\cos\theta_2-\mathbf{i}\rho\sin\theta_2|^2-(r\rho+1)^2\\ =&(1-2r\cos\theta_1+r^2)(1-2\rho\cos\theta_2+\rho^2)-(r\rho+1)^2\\ =&(r-\rho)^2-2\rho(1+r^2)\cos\theta_2-2r(1+\rho^2)\cos\theta_1+4r\rho\cos\theta_1\cos\theta_2\geqslant 0,\end{aligned}$$

hence, the lemma is valid. □

Next, the stability of the *CC-ADI-BD* scheme (2.24) and (2.14) is investigated by the Fourier analysis method.

Theorem 2.2. *The CC-ADI-BD scheme* (2.24) *and* (2.14) *is unconditionally stable with respect to the initial values and source terms, namely, it holds*

$$\|u^k\|^2 \leqslant 2\|u^0\|^2 + 2T^{2\alpha}\Gamma^2(1-\alpha)\max_{1\leqslant l\leqslant N}\|f^l\|^2, \quad 1\leqslant k\leqslant N. \tag{2.26}$$

Proof. From Eq. (2.23) and Lemma 2.3, we get

$$(1-a_x-\mathbf{i}b_x)(1-a_y-\mathbf{i}b_y)\xi^1 = (a_x+\mathbf{i}b_x)(a_y+\mathbf{i}b_y)\xi^0+\xi^0+\mu\eta^1, \tag{2.27}$$

$$\begin{aligned}(1-a_x-\mathbf{i}b_x)(1-a_y-\mathbf{i}b_y)\xi^k =& [a_0^{(\alpha)}-a_1^{(\alpha)}+(a_x+\mathbf{i}b_x)(a_y+\mathbf{i}b_y)]\xi^{k-1}\\ &+\sum_{l=1}^{k-2}(a_{k-l-1}^{(\alpha)}-a_{k-l}^{(\alpha)})\xi^l+a_{k-1}^{(\alpha)}\xi^0+\mu\eta^k,\ 2\leqslant k\leqslant N,\end{aligned} \tag{2.28}$$

where the meanings of a_x, b_x, a_y, b_y are the same as what defined in section 2.2.

For $k=1$, noticing (2.18), $|(1-a_x-\mathbf{i}b_x)(1-a_y-\mathbf{i}b_y)|\geqslant 1$ and $\mu\leqslant T^\alpha\Gamma(1-\alpha)$, we arrive at from (2.27) that

$$\begin{aligned}|\xi^1| &\leqslant \Big|\frac{1+(a_x+\mathbf{i}b_x)(a_y+\mathbf{i}b_y)}{(1-a_x-\mathbf{i}b_x)(1-a_y-\mathbf{i}b_y)}\Big||\xi^0|+\frac{\mu}{|(1-a_x-\mathbf{i}b_x)(1-a_y-\mathbf{i}b_y)|}|\eta^1|\\ &\leqslant |\xi^0|+\mu|\eta^1|\leqslant |\xi^0|+T^\alpha\Gamma(1-\alpha)|\eta^1|,\end{aligned}$$

then the square of the both sides in the above inequality yields

$$|\xi^1|^2\leqslant 2|\xi^0|^2+2T^{2\alpha}\Gamma^2(1-\alpha)|\eta^1|^2,$$

from which, it holds

$$\|u^1\|^2\leqslant 2\|u^0\|^2+2T^{2\alpha}\Gamma^2(1-\alpha)\|f^1\|^2.$$

Thus, the conclusion (2.26) holds for $k=1$.

Suppose that (2.26) is valid for $k=1,2,\ldots,n-1$. For $k=n$, by Lemma 2.2, Lemma 2.4 and $\mu\leqslant T^\alpha\Gamma(1-\alpha)a_{n-1}^{(\alpha)}$, it yields from (2.28) that

$$\begin{aligned}|\xi^n| \leqslant& \Big|\frac{a_0^{(\alpha)}-a_1^{(\alpha)}+(a_x+\mathbf{i}b_x)(a_y+\mathbf{i}b_y)}{(1-a_x-\mathbf{i}b_x)(1-a_y-\mathbf{i}b_y)}\Big||\xi^{n-1}|\\ &+\frac{1}{|(1-a_x-\mathbf{i}b_x)(1-a_y-\mathbf{i}b_y)|}\Big[\sum_{l=1}^{n-2}(a_{n-l-1}^{(\alpha)}-a_{n-l}^{(\alpha)})|\xi^l|+a_{n-1}^{(\alpha)}|\xi^0|+\mu|\eta^n|\Big]\\ \leqslant&\frac{a_0^{(\alpha)}-a_1^{(\alpha)}+|(a_x+\mathbf{i}b_x)(a_y+\mathbf{i}b_y)|}{|(1-a_x-\mathbf{i}b_x)(1-a_y-\mathbf{i}b_y)|}|\xi^{n-1}|\\ &+\frac{1}{|(1-a_x-\mathbf{i}b_x)(1-a_y-\mathbf{i}b_y)|}\Big[\sum_{l=1}^{n-2}(a_{n-l-1}^{(\alpha)}-a_{n-l}^{(\alpha)})|\xi^l|+a_{n-1}^{(\alpha)}(|\xi^0|+T^\alpha\Gamma(1-\alpha)|\eta^n|)\Big].\end{aligned}$$

Then by the Cauchy-Schwarz inequality and (2.18), the square of the above inequality gives

$$\begin{aligned}
|\xi^n|^2 \leqslant & \left\{ \frac{a_0^{(\alpha)}-a_1^{(\alpha)}+|(a_x+\mathbf{i}b_x)(a_y+\mathbf{i}b_y)|}{|(1-a_x-\mathbf{i}b_x)(1-a_y-\mathbf{i}b_y)|}|\xi^{n-1}|^2+\frac{1}{|(1-a_x-\mathbf{i}b_x)(1-a_y-\mathbf{i}b_y)|} \right. \\
& \left. \cdot \left[\sum_{l=1}^{n-2}(a_{n-l-1}^{(\alpha)}-a_{n-l}^{(\alpha)})|\xi^l|^2+a_{n-1}^{(\alpha)}(|\xi^0|+T^\alpha\Gamma(1-\alpha)|\eta^n|)^2 \right] \right\} \\
& \cdot \frac{a_0^{(\alpha)}+|(a_x+\mathbf{i}b_x)(a_y+\mathbf{i}b_y)|}{|(1-a_x-\mathbf{i}b_x)(1-a_y-\mathbf{i}b_y)|} \\
\leqslant & \frac{a_0^{(\alpha)}-a_1^{(\alpha)}+|(a_x+\mathbf{i}b_x)(a_y+\mathbf{i}b_y)|}{|(1-a_x-\mathbf{i}b_x)(1-a_y-\mathbf{i}b_y)|}|\xi^{n-1}|^2+\frac{1}{|(1-a_x-\mathbf{i}b_x)(1-a_y-\mathbf{i}b_y)|} \\
& \cdot \left[\sum_{l=1}^{n-2}(a_{n-l-1}^{(\alpha)}-a_{n-l}^{(\alpha)})|\xi^l|^2+a_{n-1}^{(\alpha)}(2|\xi^0|^2+2T^{2\alpha}\Gamma^2(1-\alpha)|\eta^n|^2) \right].
\end{aligned}$$

Hence, denoting

$$F=2\|u^0\|^2+2T^{2\alpha}\Gamma^2(1-\alpha)\max_{1\leqslant l\leqslant N}\|f^l\|^2,$$

by the induction hypothesis, further we can obtain

$$\begin{aligned}
\|u^n\|^2 \leqslant & \frac{a_0^{(\alpha)}-a_1^{(\alpha)}+|(a_x+\mathbf{i}b_x)(a_y+\mathbf{i}b_y)|}{|(1-a_x-\mathbf{i}b_x)(1-a_y-\mathbf{i}b_y)|}\|u^{n-1}\|^2+\frac{1}{|(1-a_x-\mathbf{i}b_x)(1-a_y-\mathbf{i}b_y)|} \\
& \cdot \left[\sum_{l=1}^{n-2}(a_{n-l-1}^{(\alpha)}-a_{n-l}^{(\alpha)})\|u^l\|^2+a_{n-1}^{(\alpha)}(2\|u^0\|^2+2T^{2\alpha}\Gamma^2(1-\alpha)\|f^n\|^2) \right] \\
\leqslant & \frac{a_0^{(\alpha)}-a_1^{(\alpha)}+|(a_x+\mathbf{i}b_x)(a_y+\mathbf{i}b_y)|}{|(1-a_x-\mathbf{i}b_x)(1-a_y-\mathbf{i}b_y)|}F \\
& +\frac{1}{|(1-a_x-\mathbf{i}b_x)(1-a_y-\mathbf{i}b_y)|}\left[\sum_{l=1}^{n-2}(a_{n-l-1}^{(\alpha)}-a_{n-l}^{(\alpha)})F+a_{n-1}^{(\alpha)}F \right] \\
= & \frac{a_0^{(\alpha)}+|(a_x+\mathbf{i}b_x)(a_y+\mathbf{i}b_y)|}{|(1-a_x-\mathbf{i}b_x)(1-a_y-\mathbf{i}b_y)|}F \leqslant F,
\end{aligned}$$

namely, the inequality (2.26) is also valid for $k=n$, where Lemma 2.4 is applied in the final step. By the mathematical induction method, the theorem is proved. □

Theorem 2.1 and Theorem 2.2 show that the *CC-ADI-L1* scheme (2.13)–(2.14) and *CC-ADI-BD* scheme (2.24) and (2.14) are both unconditionally stable with respect to the initial values and source terms.

3 Numerical experiments

In this section, several numerical examples are computed to demonstrate the effectiveness, convergence and the numerical accuracy of two CC-ADI schemes we present in the above work. The local truncation error of the *CC-ADI-L1* scheme is $\mathcal{O}(h^6+\tau^{\min\{2\alpha,2-\alpha\}})$, while for the *CC-ADI-BD* scheme, it is $\mathcal{O}(h^6+\tau^{\min\{1+\alpha,2-\alpha\}})$. Though the global convergence analysis for these schemes has not been available yet, the following numerical computational results show the efficiency and the global convergence of both these two schemes.

Denote

$$h_x=h_y=h,\quad E_\infty^{(p)}(h,\tau)=\max_{\substack{1\leqslant i,j\leqslant M\\ 0\leqslant k\leqslant N}}|U_{ij}^k-u_{ij}^k|,\quad E_2^{(p)}(h,\tau)=\max_{0\leqslant k\leqslant N}\|U^k-u^k\|,$$

$$rate1_{\infty,h,\tau}^{(p)}=\mathrm{Log}_2\frac{E_\infty^{(p)}(h,\tau)}{E_\infty^{(p)}(h,\tau/2)},\quad rate2_{2,h,\tau}^{(p)}=\mathrm{Log}_2\frac{E_2^{(p)}(h,\tau)}{E_2^{(p)}(h,\tau/2)},$$

$$rate3_{\infty,h,\tau}^{(p)}=\frac{\mathrm{Log}[E_\infty^{(p)}(h_1,\tau)/E_\infty^{(p)}(h_2,\tau)]}{\mathrm{Log}[h_1/h_2]},\quad rate4_{2,h,\tau}^{(p)}=\frac{\mathrm{Log}[E_2^{(p)}(h_1,\tau)/E_2^{(p)}(h_2,\tau)]}{\mathrm{Log}[h_1/h_2]},$$

Example 1

In (2.1)–(2.3), take $f(x,y,t)=[6t^{3-\alpha}/\Gamma(4-\alpha)+(\kappa_1+\kappa_2)t^3]\sin x\sin y+t^3(p\cos x\sin y+q\sin x\cos y)$, $u_0(x,y)=0$, $d_1=d_2=2\pi$.

The exact solution is given by $u(x,y,t)=t^3\sin x\sin y$.

On a bounded domain $\Omega\times[0,T]$, we compute the example using the *CC-ADI-L1* scheme (2.13)–(2.14) and the *CC-ADI-BD* scheme (2.24) together with (2.14), respectively.

Firstly, the numerical accuracy in temporal direction is tested for the case of $p=q=\kappa_1=\kappa_2=1$ and $T=1$. Taking a fixed space mesh step size $h=\pi/20$, the numerical example is computed using the *CC-ADI-L1* scheme (2.13)–(2.14) and the *CC-ADI-BD* scheme (2.24) together with (2.14), respectively, with the varying time step sizes $\tau=1/20$, $1/40$, $1/80$, $1/160$, $1/320$, $1/640$, $1/1280$. The results of the *CC-ADI-L1* scheme (2.13)–(2.14) and the *CC-ADI-BD* scheme (2.24) together with (2.14) are listed in Table 1 and Table 2, respectively, for different anomalous diffusion exponent α. It is found from Table 1 and Table 2 to be highly consistent of the global time accuracy with the local time accuracy for the above two *CC-ADI* schemes. For the *CC-ADI-L1* scheme, the numerical accuracy in time is $\min\{2\alpha,2-\alpha\}$ both in the sense of discrete maximum norm and in the discrete L_2 norm, and it is $\min\{1+\alpha,2-\alpha\}$ for the *CC-ADI-BD* scheme.

Secondly, with a sufficiently small $\tau=1/200{,}000$ and varying space mesh step size h, the numerical errors and convergence orders of both two CC-ADI schemes at $T=1$ for $p=q=\kappa_1=\kappa_2=1$ are given in Table 3 and Table 4, respectively. The small value of τ can guarantee that the dominant computational errors come from the spatial approximation. From the tables, the sixth-order high accuracy in space can be achieved for both the *CC-ADI-L1* and *CC-ADI-BD* schemes in the discrete maximum norm and in the discrete L_2 norm.

Table 1: (Ex. 1): Numerical errors and convergence orders of the *CC-ADI-L1* scheme (2.13)–(2.14) in temporal direction with a fixed $h=\pi/20$.

	τ	$E_{\infty}^{(p)}(h,\tau)$	$rate1_{\infty,h,\tau}^{(p)}$	$E_{2}^{(p)}(h,\tau)$	$rate2_{2,h,\tau}^{(p)}$
	1/20	1.131470×10^{-2}	1.32	3.976601×10^{-2}	1.31
	1/40	4.535128×10^{-3}	1.33	1.601624×10^{-2}	1.32
	1/80	1.805164×10^{-3}	1.33	6.397647×10^{-3}	1.33
$\alpha=2/3$	1/160	7.167760×10^{-4}	1.33	2.546434×10^{-3}	1.33
	1/320	2.844000×10^{-4}	1.33	1.011965×10^{-3}	1.33
	1/640	1.128273×10^{-4}	1.33	4.018752×10^{-4}	1.33
	1/1280	4.476274×10^{-5}	—	1.595404×10^{-4}	—
	1/20	3.269260×10^{-2}	0.95	1.029403×10^{-1}	0.95
	1/40	1.687157×10^{-2}	0.97	5.315399×10^{-2}	0.97
	1/80	8.596133×10^{-3}	0.98	2.711039×10^{-2}	0.98
$\alpha=1/2$	1/160	4.348405×10^{-3}	0.99	1.372878×10^{-2}	0.99
	1/320	2.190438×10^{-3}	0.99	6.922193×10^{-3}	0.99
	1/640	1.100577×10^{-3}	1.00	3.480682×10^{-3}	0.99
	1/1280	5.521886×10^{-4}	—	1.747062×10^{-3}	—
	1/20	8.221316×10^{-2}	0.62	2.586591×10^{-1}	0.62
	1/40	5.339284×10^{-2}	0.64	1.681582×10^{-1}	0.64
	1/80	3.426042×10^{-2}	0.65	1.079911×10^{-1}	0.65
$\alpha=1/3$	1/160	2.182628×10^{-2}	0.66	6.883928×10^{-2}	0.66
	1/320	1.384467×10^{-2}	0.66	4.368364×10^{-2}	0.66
	1/640	8.758690×10^{-3}	0.66	2.764361×10^{-2}	0.66
	1/1280	5.532142×10^{-3}	—	1.746332×10^{-2}	—

In Figure 1, for $p=q=\kappa_1=\kappa_2=1$, the exact solution and numerical solutions are all displayed for $\alpha=2/3$ with $N=200$, $M_1=M_2=100$ at $T=1$. The close agreement between the exact solution and numerical solutions shows that the proposed methods perform well and they are both reliable in solving the example.

Finally, the comparison of computational efficiency between our *CC-ADI-BD* scheme and *Scheme 1* in [20], which own the same temporal discretization accuracy, is illustrated. With $\kappa_1=\kappa_2=1$, $p=q=0$, $T=1$ and $\alpha=1/2$, the optimal step sizes are chosen to keep the computational errors of these two difference schemes on the same magnitude, i.e. $\tau^{1.5}\approx h^k$ ($k=6$ for our *CC-ADI-BD* scheme, and $k=4$ for *Scheme 1* in [20]). Table 5 displays the involved mesh numbers, the maximum errors and the consuming CPU time on the same machine. The advantage of the *CC-ADI-BD* scheme over the latter can be observed.

Example 2

In (2.1)–(2.3), take $f(x,y,t)=\cos(x+y)[-t^{1-\alpha}E_{1,2-\alpha}(-t)+2\exp(-t)]-2\exp(-t)\sin(x+y)$, $u_0(x,y)=\cos(x+y)$, $p=q=\kappa_1=\kappa_2=1$, $d_1=d_2=2\pi$, where $E_{\beta,\gamma}(z)$ is the Mittag-Leffler

Table 2: (Ex. 1): Numerical errors and convergence orders of the *CC-ADI-BD* scheme (2.24) and (2.14) in temporal direction with a fixed $h=\pi/20$.

	τ	$E_{\infty}^{(p)}(h,\tau)$	$rate1_{\infty,h,\tau}^{(p)}$	$E_{2}^{(p)}(h,\tau)$	$rate2_{2,h,\tau}^{(p)}$
	1/20	6.494117×10^{-3}	1.22	2.694366×10^{-2}	1.39
	1/40	2.778851×10^{-3}	1.24	1.024768×10^{-2}	1.35
	1/80	1.173784×10^{-3}	1.25	4.019246×10^{-3}	1.32
$\alpha=2/3$	1/160	4.922575×10^{-4}	1.27	1.610701×10^{-3}	1.30
	1/320	2.034615×10^{-4}	1.29	6.522810×10^{-4}	1.30
	1/640	8.323678×10^{-5}	1.29	2.649495×10^{-4}	1.30
	1/1280	3.395574×10^{-5}	—	1.075249×10^{-4}	—
	1/20	1.278439×10^{-2}	1.45	4.052883×10^{-2}	1.45
	1/40	4.666796×10^{-3}	1.48	1.479754×10^{-2}	1.48
	1/80	1.673930×10^{-3}	1.49	5.309498×10^{-3}	1.49
$\alpha=1/2$	1/160	5.956025×10^{-4}	1.50	1.889821×10^{-3}	1.50
	1/320	2.111422×10^{-4}	1.50	6.701441×10^{-4}	1.50
	1/640	7.472620×10^{-5}	1.50	2.372302×10^{-4}	1.50
	1/1280	2.642769×10^{-5}	—	8.391405×10^{-5}	—
	1/20	2.487747×10^{-2}	1.27	7.856964×10^{-2}	1.27
	1/40	1.030182×10^{-2}	1.30	3.254185×10^{-2}	1.30
	1/80	4.181260×10^{-3}	1.32	1.320688×10^{-2}	1.32
$\alpha=1/3$	1/160	1.680452×10^{-3}	1.32	5.307097×10^{-3}	1.32
	1/320	6.719982×10^{-4}	1.33	2.121981×10^{-3}	1.33
	1/640	2.680052×10^{-4}	1.33	8.461963×10^{-4}	1.33
	1/1280	1.067217×10^{-4}	—	3.369356×10^{-4}	—

Table 3: (Ex. 1): Errors and convergence orders of the *CC-ADI-L1* scheme (2.13)–(2.14) in spatial direction with $\tau=1/200{,}000$ ($\alpha=2/3$).

$M_1=M_2$	$E_{\infty}^{(p)}(h,\tau)$	$rate3_{\infty,h,\tau}^{(p)}$	$E_{2}^{(p)}(h,\tau)$	$rate4_{2,h,\tau}^{(p)}$
4	1.558950×10^{-3}	5.93	6.977905×10^{-3}	6.27
8	2.552192×10^{-5}	5.83	9.058593×10^{-5}	6.10
12	2.403109×10^{-6}	6.13	7.639662×10^{-6}	6.14
16	4.122885×10^{-7}	—	1.304184×10^{-6}	—

function with two parameters defined by

$$E_{\beta,\gamma}(z)=\sum_{k=0}^{+\infty}\frac{z^k}{\Gamma(\beta k+\gamma)}.$$

The exact solution is given by $u(x,y,t)=\exp(-t)\cos(x+y)$.
On a bounded domain $\Omega\times[0,T]$, we compute the example using the *CC-ADI-L1* scheme

Table 4: (Ex.1): Errors and convergence orders of the *CC-ADI-BD* scheme (2.24) and (2.14) in spatial direction with $\tau = 1/200{,}000$ ($\alpha = 1/2$).

$M_1 = M_2$	$E_\infty^{(p)}(h,\tau)$	$rate3_{\infty,h,\tau}^{(p)}$	$E_2^{(p)}(h,\tau)$	$rate4_{2,h,\tau}^{(p)}$
4	1.667372×10^{-3}	5.86	7.675144×10^{-3}	6.26
8	2.868772×10^{-5}	5.84	9.990945×10^{-5}	6.08
12	2.687925×10^{-6}	6.02	8.494229×10^{-6}	6.03
16	4.761564×10^{-7}	—	1.498762×10^{-6}	—

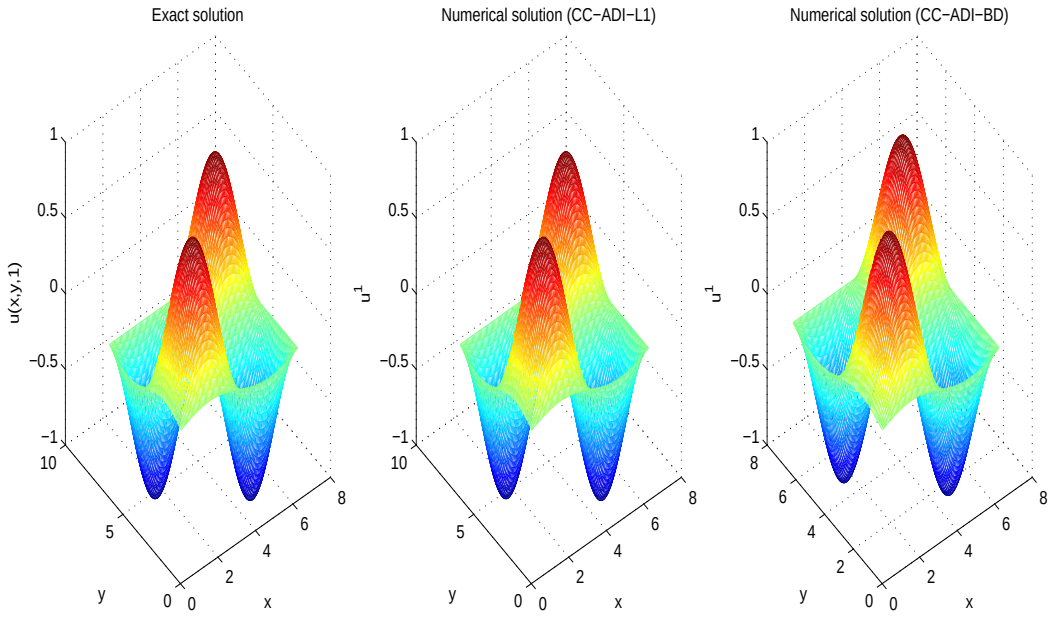

Figure 1: (Ex.1) The solution surfaces at $T = 1$ with $\alpha = 2/3$, $N = 200$, $M_1 = M_2 = 100$ and $p = q = \kappa_1 = \kappa_2 = 1$ (Left: Exact solution; Middle: the solution of *CC-ADI-L1* scheme; Right: the solution of *CC-ADI-BD* scheme)

(2.13)–(2.14) and the *CC-ADI-BD* scheme (2.24) together with (2.14), respectively. The numerical accuracy of the new presented two CC-ADI schemes for computing the example is tested.

Firstly, the temporal accuracy is numerically examined. With a fixed, sufficiently small spatial step size $h = \pi/20$ and varying temporal step sizes, the computational results for $T = 1$ using the *CC-ADI-L1* scheme (2.13)–(2.14) and the *CC-ADI-BD* scheme (2.24) together with (2.14), are displayed in Table 6 and Table 7, respectively. The close agreement of the global convergence orders with the local truncation error orders can be concluded from the numerical results.

Table 5: (Ex.1): The comparison between the *CC-ADI-BD* scheme and the *Scheme 1* in [20] for $\alpha = 1/2$ and $M_1 = M_2 = M$.

N	*CC-ADI-BD* scheme			*Scheme 1* in [20]		
	M	$E_\infty^{(p)}(h,\tau)$	CPU time (s)	M	$E_\infty^{(p)}(h,\tau)$	CPU time (s)
32	15	1.7178×10^{-3}	1.0291	58	1.7306×10^{-3}	11.0650
103	20	3.0259×10^{-4}	4.4935	90	3.0205×10^{-4}	95.5454
251	25	7.8662×10^{-5}	17.2056	125	7.8915×10^{-5}	565.2670
520	30	2.6024×10^{-5}	53.0401	164	2.6296×10^{-5}	2844.8843
963	35	1.0368×10^{-5}	169.1300	207	1.0383×10^{-5}	12472.3761

Table 6: (Ex. 2): Numerical errors and convergence orders of the *CC-ADI-L1* scheme (2.13)–(2.14) in temporal direction with a fixed $h = \pi/20$.

	τ	$E_\infty^{(p)}(h,\tau)$	$rate1_{\infty,h,\tau}^{(p)}$	$E_2^{(p)}(h,\tau)$	$rate2_{2,h,\tau}^{(p)}$
	1/20	3.395149×10^{-3}	1.41	1.509142×10^{-2}	1.41
	1/40	1.281104×10^{-3}	1.35	5.698244×10^{-3}	1.35
	1/80	5.024710×10^{-4}	1.30	2.237659×10^{-3}	1.30
$\alpha = 4/5$	1/160	2.046658×10^{-4}	1.26	9.104348×10^{-4}	1.26
	1/320	8.559203×10^{-5}	1.24	3.802782×10^{-4}	1.23
	1/640	3.627098×10^{-5}	1.22	1.616018×10^{-4}	1.22
	1/1280	1.561923×10^{-5}	—	6.940080×10^{-5}	—
	1/20	1.412687×10^{-2}	0.99	6.278748×10^{-2}	0.99
	1/40	7.108387×10^{-3}	1.00	3.158469×10^{-2}	1.00
	1/80	3.566203×10^{-3}	1.00	1.584445×10^{-2}	1.00
$\alpha = 1/2$	1/160	1.786325×10^{-3}	1.00	7.936431×10^{-3}	1.00
	1/320	8.940362×10^{-4}	1.00	3.972118×10^{-3}	1.00
	1/640	4.472589×10^{-4}	1.00	1.987147×10^{-3}	1.00
	1/1280	2.236973×10^{-4}	—	9.938838×10^{-4}	—
	1/20	3.867163×10^{-2}	0.65	1.718403×10^{-1}	0.65
	1/40	2.468269×10^{-2}	0.65	1.096623×10^{-1}	0.65
	1/80	1.567613×10^{-2}	0.66	6.965249×10^{-2}	0.66
$\alpha = 1/3$	1/160	9.925551×10^{-3}	0.66	4.410654×10^{-2}	0.66
	1/320	6.272562×10^{-3}	0.66	2.787641×10^{-2}	0.66
	1/640	3.959326×10^{-3}	0.66	1.759726×10^{-2}	0.66
	1/1280	2.497331×10^{-3}	—	1.109997×10^{-2}	—

Secondly, the spatial accuracy is tested. Taking a sufficiently small temporal step size $\tau = 1/200{,}000$, for $T = 1$, the example is computed with the *CC-ADI-L1* scheme (2.13)–(2.14) and the *CC-ADI-BD* scheme (2.24) together with (2.14), respectively. The computational errors in both the discrete maximum norm and the discrete L_2 norm, and the numerical convergence orders are recorded in Table 8 and Table 9. The spatial sixth-order convergence

Table 7: (Ex. 2): Numerical errors and convergence orders of the *CC-ADI-BD* scheme (2.24) and (2.14) in temporal direction with a fixed $h=\pi/20$.

	τ	$E_{\infty}^{(p)}(h,\tau)$	$rate1_{\infty,h,\tau}^{(p)}$	$E_{2}^{(p)}(h,\tau)$	$rate2_{2,h,\tau}^{(p)}$
	1/20	2.810742×10^{-3}	1.36	1.248886×10^{-2}	1.36
	1/40	1.097339×10^{-3}	1.28	4.877497×10^{-3}	1.28
	1/80	4.509777×10^{-4}	1.24	2.004074×10^{-3}	1.24
$\alpha=4/5$	1/160	1.910147×10^{-4}	1.22	8.488613×10^{-4}	1.22
	1/320	8.205808×10^{-5}	1.21	3.650071×10^{-4}	1.21
	1/640	3.552523×10^{-5}	1.20	1.580413×10^{-4}	1.20
	1/1280	1.544532×10^{-5}	—	6.863504×10^{-5}	—
	1/20	4.148883×10^{-3}	1.48	1.843395×10^{-2}	1.48
	1/40	1.482320×10^{-3}	1.49	6.585773×10^{-3}	1.49
	1/80	5.260278×10^{-4}	1.50	2.337083×10^{-3}	1.50
$\alpha=1/2$	1/160	1.862292×10^{-4}	1.50	8.273952×10^{-4}	1.50
	1/320	6.587420×10^{-5}	1.50	2.926715×10^{-4}	1.50
	1/640	2.329443×10^{-5}	1.50	1.034944×10^{-4}	1.50
	1/1280	8.236642×10^{-6}	—	3.659444×10^{-5}	—
	1/20	7.126250×10^{-3}	1.31	3.175127×10^{-2}	1.32
	1/40	2.866529×10^{-3}	1.33	1.275642×10^{-2}	1.33
	1/80	1.142603×10^{-3}	1.33	5.082520×10^{-3}	1.33
$\alpha=1/3$	1/160	4.541809×10^{-4}	1.33	2.020103×10^{-3}	1.33
	1/320	1.803655×10^{-4}	1.33	8.020851×10^{-4}	1.33
	1/640	7.159832×10^{-5}	1.33	3.183637×10^{-4}	1.33
	1/1280	2.841790×10^{-5}	—	1.263511×10^{-4}	—

of these two CC-ADI schemes is verified by the example.

Table 8: (Ex. 2): Errors and convergence orders of the *CC-ADI-L1* scheme (2.13)–(2.14) in spatial direction with $\tau=1/200{,}000$ ($\alpha=2/3$).

$M_1=M_2$	$E_{\infty}^{(p)}(h,\tau)$	$rate3_{\infty,h,\tau}^{(p)}$	$E_{2}^{(p)}(h,\tau)$	$rate4_{2,h,\tau}^{(p)}$
4	2.225246×10^{-3}	6.28	1.060663×10^{-2}	6.36
8	2.867901×10^{-5}	6.07	1.293454×10^{-4}	6.10
12	2.444373×10^{-6}	6.05	1.091675×10^{-5}	6.02
16	4.285131×10^{-7}	—	1.933598×10^{-6}	—

Example 3

Compute the problem

$$ {}_{0}^{C}\mathcal{D}_{t}^{\alpha}u(x,y,t)=\Delta u(x,y,t),\quad (x,y)\in\mathbb{R}^2,\ t\in(0,T], \tag{3.1}$$

Table 9: (Ex. 2): Errors and convergence orders of the *CC-ADI-BD* scheme (2.24) and (2.14) in spatial direction with $\tau = 1/200{,}000$ ($\alpha = 1/2$).

$M_1 = M_2$	$E_{\infty}^{(p)}(h,\tau)$	$rate3_{\infty,h,\tau}^{(p)}$	$E_{2}^{(p)}(h,\tau)$	$rate4_{2,h,\tau}^{(p)}$
4	2.210411×10^{-3}	6.27	1.058854×10^{-2}	6.36
8	2.863993×10^{-5}	6.08	1.290847×10^{-4}	6.10
12	2.432288×10^{-6}	6.05	1.088113×10^{-5}	6.04
16	4.270375×10^{-7}	—	1.913866×10^{-6}	—

$$u(x,y,0) = \cos(\frac{\pi}{2}x)\sin(\frac{\pi}{2}y), \quad (x,y) \in \mathbb{R}^2, \tag{3.2}$$

subject to the $(4,4)$-periodic boundary conditions

$$u(x,y,t) = u(x+4,y,t),\ u(x,y,t) = u(x,y+4,t) \quad (x,y) \in \mathbb{R}^2,\ t \in [0,T]. \tag{3.3}$$

The problem is in fact a sub-diffusion problem. On a periodic domain $\Omega = (0,4]^2$, we compute the example using the *CC-ADI-L1* scheme (2.13)–(2.14) and the *CC-ADI-BD* scheme (2.24) together with (2.14), respectively. For simplicity, let $M_1 = M_2 = M$ and $h_x = h_y = h$. For $T = 1$, the numerical solutions are computed.

The exact solution of the example is given by [16]

$$u(x,y,t) = E_{\alpha,1}\Big(-\frac{\pi^2}{2}t^{\alpha}\Big)\cos(\frac{\pi}{2}x)\sin(\frac{\pi}{2}y).$$

Due to the fact that the exact solution is not smooth enough in the temporal variable, the anticipated numerical accuracy of the above proposed schemes is not achieved longer. Next, we would like to test the efficiency of the proposed CC-ADI schemes for solving this non-smooth enough problem. When $T = 1$, Table 10 and Table 11 report the numerical values of solutions at some randomly selected mesh points using the *CC-ADI-L1* scheme (2.13)–(2.14) for $\alpha = 1/2$. For comparison, the exact values are listed in the last line. One can see that the numerical solutions are convergent to the exact ones. The computational results using the *CC-ADI-BD* scheme (2.24) together with (2.14) for $\alpha = 1/2$ are given in Table 12 and Table 13. The similar conclusion can be drawn. Thus, the convergence of these two CC-ADI schemes for this non-smooth enough problem is verified.

4 Conclusion

Two three-point CC-ADI schemes, called the *CC-ADI-L1* scheme and *CC-ADI-BD* scheme, respectively, are developed for solving a class of two-dimensional time-fractional advection-diffusion equations. The high-order numerical accuracy in space is achieved for both these two schemes. Their unconditional stabilities are proved by the Fourier method. Several numerical experiments are carried out to illustrate the efficiency and spatial high-order

Table 10: (Ex. 3): Numerical solutions of Example 4 at $T=1$ using the *CC-ADI-L1* scheme (2.13)–(2.14) ($\alpha=1/2$).

τ	h	(0.8,1.2)	(0.8,1.6)	(4,1.2)	(2,2)	(3.2,1.2)	(2,3.6)
1/20	4/10	0.04095020	0.02530862	0.13251764	−0.00000000	0.04095020	0.08190041
1/40	4/20	0.03694654	0.02283422	0.11956152	−0.00000000	0.03694654	0.07389308
1/80	4/30	0.03494669	0.02159824	0.11308985	−0.00000000	0.03494669	0.06989337
1/160	4/40	0.03394752	0.02098072	0.10985648	−0.00000000	0.03394752	0.06789504
1/320	4/50	0.03344819	0.02067212	0.10824063	−0.00000000	0.03344819	0.06689639
1/640	4/60	0.03319862	0.02051788	0.10743300	−0.00000000	0.03319862	0.06639724
1/1280	4/70	0.03307387	0.02044077	0.10702928	−0.00000000	0.03307387	0.06614774
1/2560	4/80	0.03301150	0.02040223	0.10682746	−0.00000000	0.03301150	0.06602300
1/5120	4/90	0.03298032	0.02038296	0.10672656	−0.00000000	0.03298032	0.06596064
1/10240	4/100	0.03296473	0.02037333	0.10667612	0.00000000	0.03296473	0.06592947
exact		0.03294915	0.02036369	0.10662568	0.00000000	0.03294915	0.06589830

Table 11: (Ex. 3): Numerical solutions of Example 4 at $T=1$ using the *CC-ADI-L1* scheme (2.13)–(2.14) with a fixed $h=\pi/30$ ($\alpha=1/2$).

τ	(0.8,1.2)	(0.8,1.6)	(4,1.2)	(2,2)	(3.2,1.2)	(2,3.6)
1/20	0.04095058	0.02530885	0.13251886	−0.00000000	0.04095058	0.08190116
1/40	0.03694655	0.02283422	0.11956154	−0.00000000	0.03694655	0.07389309
1/80	0.03494669	0.02159824	0.11308985	−0.00000000	0.03494669	0.06989337
1/160	0.03394752	0.02098072	0.10985648	0.00000000	0.03394752	0.06789504
1/320	0.03344819	0.02067212	0.10824063	−0.00000000	0.03344819	0.06689639
1/640	0.03319862	0.02051788	0.10743300	−0.00000000	0.03319862	0.06639724
1/1280	0.03307387	0.02044077	0.10702928	−0.00000000	0.03307387	0.06614774
1/2560	0.03301150	0.02040223	0.10682746	−0.00000000	0.03301150	0.06602300
1/5120	0.03298032	0.02038296	0.10672656	0.00000000	0.03298032	0.06596064
1/10240	0.03296473	0.02037333	0.10667612	−0.00000000	0.03296473	0.06592947
1/20480	0.03295694	0.02036851	0.10665090	−0.00000000	0.03295694	0.06591388
1/40960	0.03295304	0.02036610	0.10663829	−0.00000000	0.03295304	0.06590609
exact	0.03294915	0.02036369	0.10662568	0.00000000	0.03294915	0.06589830

accuracy of the proposed schemes. It is worth noting that if α is close to 1, the lower-order numerical accuracy in time of these two CC-ADI schemes can be encountered. Then the combination of the CCD techniques and the alternating direction treatment developed in [22] for the equivalent Riemann-Liouville type equations can be considered. Rigorous convergence analysis of the mentioned schemes and improvement on the overall numerical accuracy are still open and will be our future work.

Table 12: (Ex. 3): Numerical solutions of Example 4 at $T=1$ using the *CC-ADI-BD* scheme (2.24) and (2.14) ($\alpha=1/2$).

τ	h	(0.8,1.2)	(0.8,1.6)	(4,1.2)	(2,2)	(3.2,1.2)	(2,3.6)
1/20	4/10	0.03378448	0.02087996	0.10932888	−0.00000000	0.03378448	0.06756896
1/40	4/20	0.03329344	0.02057648	0.10773984	−0.00000000	0.03329344	0.06658689
1/80	4/30	0.03309846	0.02045597	0.10710886	−0.00000000	0.03309846	0.06619692
1/160	4/40	0.03301620	0.02040514	0.10684268	−0.00000000	0.03301620	0.06603241
1/320	4/50	0.03298007	0.02038280	0.10672574	−0.00000000	0.03298007	0.06596013
1/640	4/60	0.03296370	0.02037269	0.10667277	−0.00000000	0.03296370	0.06592740
1/1280	4/70	0.03295610	0.02036799	0.10664820	−0.00000000	0.03295610	0.06591221
1/2560	4/80	0.03295251	0.02036577	0.10663658	−0.00000000	0.03295251	0.06590503
1/5120	4/90	0.03295079	0.02036471	0.10663100	−0.00000000	0.03295079	0.06590158
1/10240	4/100	0.03294996	0.02036419	0.10662830	0.00000000	0.03294996	0.06589991
exact		0.03294915	0.02036369	0.10662568	0.00000000	0.03294915	0.06589830

Table 13: (Ex. 3): Numerical solutions of Example 4 at $T=1$ using the *CC-ADI-BD* scheme (2.24) and (2.14) with a fixed $h=\pi/30$ ($\alpha=1/2$).

τ	(0.8,1.2)	(0.8,1.6)	(4,1.2)	(2,2)	(3.2,1.2)	(2,3.6)
1/20	0.03378499	0.02088027	0.10933053	−0.00000000	0.03378499	0.06756998
1/40	0.03329345	0.02057648	0.10773987	−0.00000000	0.03329345	0.06658690
1/80	0.03309846	0.02045597	0.10710886	−0.00000000	0.03309846	0.06619692
1/160	0.03301620	0.02040514	0.10684268	0.00000000	0.03301620	0.06603241
1/320	0.03298007	0.02038280	0.10672574	−0.00000000	0.03298007	0.06596013
1/640	0.03296370	0.02037269	0.10667277	−0.00000000	0.03296370	0.06592740
1/1280	0.03295610	0.02036799	0.10664820	−0.00000000	0.03295610	0.06591221
1/2560	0.03295251	0.02036577	0.10663658	−0.00000000	0.03295251	0.06590503
1/5120	0.03295079	0.02036471	0.10663100	0.00000000	0.03295079	0.06590158
1/10240	0.03294996	0.02036419	0.10662830	−0.00000000	0.03294996	0.06589991
exact	0.03294915	0.02036369	0.10662568	0.00000000	0.03294915	0.06589830

Acknowledgments

The research was supported by the research grant 11271068, 11326225, 11401319 from National Natural Science Foundation of China, BK20130860 from Natural Science Youth Foundation of Jiangsu Province, NY213051 from the Scientific Research Foundation of Nanjing University of Posts and Telecommunications, 105/2012/A3 from FDCT of Macao, and MYRG102(Y2-L3)-FST13-SHW from University of Macau.

The authors would like to show their deep gratitude to the anonymous referees for their invaluable suggestions and comments to improve the manuscript.

References

[1] V. Uchaikin, Fractional Derivatives for Physicists and Engineers, Higher Education Press, Beijing, 2013.
[2] I. Podlubny, Fractional Differential Equations, Academic Press, San Diego, 1999.
[3] A. Kilbas, H. Srivastava and J. Trujillo, Theory and Applications of Fractional Differential Equations, Elsevier Science and Technology, Boston, 2006.
[4] S. Yuste and L. Acedo, An explicit finite difference method and a new von Neumann-type stability analysis for fractional diffusion equations, SIAM J. Numer. Anal., 42 (2005), 1862–1874.
[5] T. Langlands and B. Henry, The accuracy and stability of an implicit solution method for the fractional diffusion equation, J. Comput. Phys., 205 (2005), 719–736.
[6] C. Chen, F. Liu, I. Turner and V. Anh, A Fourier method for the fractional diffusion equation describing sub-diffusion, J. Comput. Phys., 227 (2007), 886–897.
[7] Z.Z. Sun, X. Wu, A fully discrete difference scheme for a diffusion-wave system, Appl. Numer. Math., 56 (2006), 193–209.
[8] M. Cui, Compact finite difference method for the fractional diffusion equation, J. Comput. Phys., 228 (2009), 7792–7804.
[9] G.H. Gao and Z.Z. Sun, A compact finite difference scheme for the fractional sub-diffusion equations, J. Comput. Phys., 230 (2011), 586–595.
[10] Y. Zhang, Z.Z. Sun and H. Wu, Error estimates of Crank-Nicolson-type difference schemes for the subdiffusion equation, SIAM J. Numer. Anal., 49 (2011), 2302–2322.
[11] A. Mohebbi and M. Abbaszadeh, Compact finite difference scheme for the solution of time fractional advection-dispersion equation, Numer. Algor., 63 (2013), 431–452.
[12] R. Du, W. Cao and Z.Z. Sun, A compact difference scheme for the fractional diffusion-wave equation, Appl. Math. Model., 34 (2010), 2998–3007.
[13] X. Hu and L. Zhang, A compact finite difference scheme for the fourth-order fractional diffusion-wave system, Comput. Phys. Comm., 182 (2011), 1645–1650.
[14] J. Ren and Z.Z. Sun, Numerical algorithm with high spatial accuracy for the fractional diffusion-wave equation with Neumann boundary conditions, J. Sci. Comput., 56 (2013), 381–408.
[15] Y. Lin and C. Xu, Finite difference/spectral approximations for the time-fractional diffusion equation, J. Comput. Phys., 225 (2007), 1533–1552.
[16] H. Brunner, L. Ling and M. Yamamoto, Numerical simulations of 2D fractional subdiffusion problems, J. Comput. Phys., 229 (2010), 6613–6622.
[17] C. Chen, F. Liu, I. Turner and V. Anh, Numerical schemes and multivariate extrapolation of a two-dimensional anomalous sub-diffusion equation, Numer. Algor., 54 (2010), 1–21.
[18] Y. Zhang and Z.Z. Sun, Alternating direction implicit schemes for the two-dimensional fractional sub-diffusion equation, J. Comput. Phys., 230 (2011), 8713–8728.
[19] M. Cui, Compact alternating direction implicit method for two-dimensional time fractional diffusion equation, J. Comput. Phys., 231 (2012), 2621–2633.
[20] M. Cui, Convergence analysis of high-order compact alternating direction implicit schemes for the two-dimensional time fractional diffusion equation, Numer. Algor., 62 (2013), 383–409.
[21] Y. Zhang, Z.Z. Sun and X. Zhao, Compact alternating direction implicit scheme for the two-dimensional fractional diffusion-wave equation, SIAM J. Numer. Anal., 50 (2012), 1535–1555.
[22] Y. Zhang and Z.Z. Sun, Error analysis of a compact ADI scheme for the 2D fractional subdiffusion equation, J. Sci. Comput., 59 (2014), 104–128.
[23] P. Chu, C. Fan, A three-point combined compact difference scheme, J. Comput. Phys., 140

(1998), 370–399.
[24] M. Mousa, A. Abadeer and M. Abbas, Combined compact finite difference treatment of Burgers' equation, Int. J. Pure Appl. Math., 75 (2012), 169–184.
[25] W. Chen and J. Chen, Combined compact difference method for solving the incompressible Navier-Stokes equations, Int. J. Numer. Meth. Fluids, 68 (2012), 1234–1256.
[26] F. Takahashi, Implementation of a high-order combined compact difference scheme in problems of thermally driven convection and dynamo in rotating spherical shells, Geophys. Astrophys. Fluid Dyn., 106 (2012), 231–249.
[27] H. Sun and L. Li, A CCD-ADI method for unsteady convection-diffusion equations, Comput. Phys. Comm., 185 (2014), 790–797.
[28] P. Chu and C. Fan, A three-point sixth-order nonuniform combined compact difference scheme, J. Comput. Phys., 148 (1999), 663–764.
[29] P. Chu and C. Fan, A three-point sixth-order staggered combined compact difference scheme, Math. Comput. Modelling, 32 (2000), 323–340.
[30] T. Nihei and K. Ishii, A fast solver of the shallow water equations on a sphere using a combined compact difference scheme, J. Comput. Phys., 187 (2003), 639–659.
[31] T. Sengupta, V. Vijay and S. Bhaumik, Further improvement and analysis of CCD scheme: Dissipation discretization and de-aliasing properties, J. Comput. Phys., 228 (2009), 6150–6168.
[32] G.H. Gao and H. Sun, Three-point combined compact difference schemes for time-fractional advection-diffusion equations, *submitted to* J. Comput. Phys., (2013).